

ChemComm

Accepted Manuscript



This is an *Accepted Manuscript*, which has been through the Royal Society of Chemistry peer review process and has been accepted for publication.

Accepted Manuscripts are published online shortly after acceptance, before technical editing, formatting and proof reading. Using this free service, authors can make their results available to the community, in citable form, before we publish the edited article. We will replace this *Accepted Manuscript* with the edited and formatted *Advance Article* as soon as it is available.

You can find more information about *Accepted Manuscripts* in the [Information for Authors](#).

Please note that technical editing may introduce minor changes to the text and/or graphics, which may alter content. The journal's standard [Terms & Conditions](#) and the [Ethical guidelines](#) still apply. In no event shall the Royal Society of Chemistry be held responsible for any errors or omissions in this *Accepted Manuscript* or any consequences arising from the use of any information it contains.

Humic acid as promising organic anodes for lithium/sodium ion batteries

Received 00th January 20xx,
Accepted 00th January 20xx

Hui Zhu,^{a, †} Jiao Yin,^{b, †} Xue Zhao,^a Chuanyi Wang^b and Xiurong Yang^{a, *}

DOI: 10.1039/x0xx00000x

www.rsc.org/

As a representative natural polymer with abundant functionalities, humic acid was creatively explored as anode materials for lithium ion batteries and sodium ion batteries with high storage capacitances, satisfactory cycling stabilities. Most impressively, this work oriented a promising and effective strategy for developing organic energy storage devices from natural sources.

More recently, much attention has been paid to organic compounds (organics or polymers) as electrode materials for rechargeable batteries (both lithium-ion batteries (LIBs) and sodium-ion batteries (SIBs)) due to their resource abundance, structure diversity, chemical and physical stability and mechanical softness.¹ Most importantly, by virtue of the redox reaction mechanism, theoretical capacities and reaction rates of these organic materials are even higher than that of inorganic intercalation compounds, endowing them with high energy and power density.

Until now, most organic materials, including organosulfur materials,² free radical compounds,³ conducting polymers⁴ and quinine-type carbonyl compounds⁵ have been presented for cathode materials with redox potentials above 2V vs Li⁺/Li or Na⁺/Na. However, compared to the blooming exploration in organic cathodes, the progress in developing organic anode is sluggish. Even though several carbonyl-based organics with small molecular weight, including conjugated dicarboxylate,⁶ 2, 6-naphthalene dicarboxylate dilithium,⁷ perylenetetracarboxylates,⁸ lithium and sodium terephthalate,⁹ Li₄C₈H₂O₆ nanosheets¹⁰ have been demonstrated as potential anode materials for LIBs or SIBs, the further enhancements in capacitance, the improvements in the rate

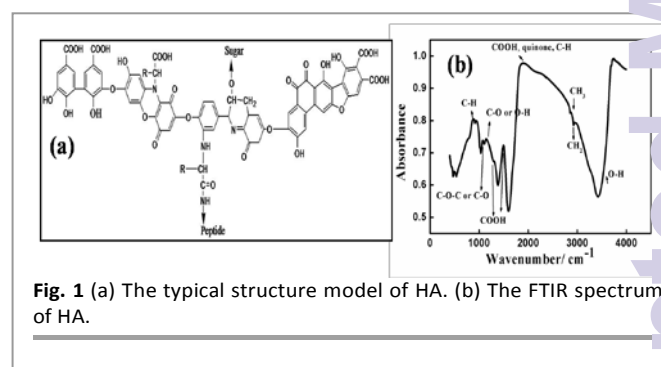


Fig. 1 (a) The typical structure model of HA. (b) The FTIR spectrum of HA.

capability and long cycling performance of them are still urgent needed. On the other hand, it has to be mentioned that most of the reported organics were derived from chemical feedstock with the high cost issues and environmental concerns. Therefore, it is a challenging task to exploring promising organic anode materials especially from environmental benign species.

In this contribution, inspired by our previous research on biomass derived carbons,¹¹ a natural polymer, humic acid (HA), which can be derived from woods, soils or coals,¹² was creatively chosen as anode materials for LIBs and SIBs. By virtue of the abundant existence of the oxygen functionalities (carboxyl, phenolic, quinone and ketone groups) in HA framework, the as-prepared anodes presented excellent storage performance, including satisfactory storage capacity, improved rate capability as well as excellent cycling behaviours.

Fig. 1a shows the typical structure model of HA. It is found that the HA molecule contains a large concentration of chemically reactive oxygen groups, including carboxyl, phenolic and alcoholic hydroxyls, which can also be confirmed by the FTIR spectra collection (Fig. 1b). In detail, the broad peak locating at 3400 cm⁻¹ belongs to O-H stretching vibration. The weak shoulders at 2914 and 2852 cm⁻¹ may be attributed to aliphatic C-H stretching of alkyl groups and stretching of methyl C-H groups. The peaks lying in 1600-2000 cm⁻¹ may be ascribed to aromatic C-H stretching, hydrogen-bonding quinone and carboxyl groups, respectively. The peaks at 1580 and 1380 cm⁻¹ may be indexed to carboxyl asymmetric stretching and symmetric stretching modes respectively. The peak at 1200 cm⁻¹ is resulted from C-O stretching and O-H deformation.

^a State Key Laboratory of Electroanalytical Chemistry, Changchun Institute of Applied Chemistry, Chinese Academy of Sciences, 5625 Renmin Street, Changchun 130022, China.

^b Key Laboratory of Functional Materials and Devices for Special Environments, Xinjiang Technical Institute of Physics & Chemistry, Chinese Academy of Sciences, 40-1 South Beijing Road, Urumqi, Xinjiang 830011, China.

* Corresponding author: Tel.: 86-431-85262056. Fax: 86-431-85689278. E-mail address: xryang@ciac.ac.cn (Prof. Xiurong Yang)

[†] These authors contributed equally to this work.

[‡] Electronic Supplementary Information (ESI) available: [Detailed experimental section is included]. See DOI: 10.1039/x0xx00000x

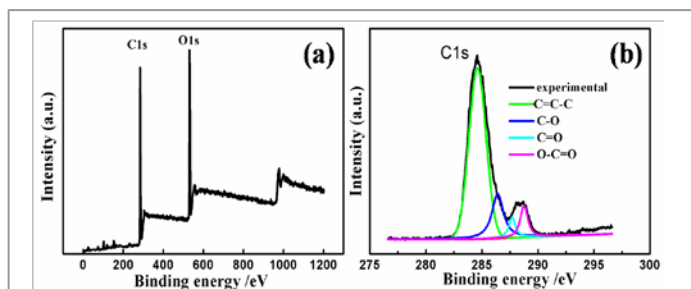


Fig. 2 (a) XPS survey scans of HA. (b) High-resolution XPS survey scans of C_{1s} peak.

Table 1. Surface chemistry analysis of HA using Boehm's titration method.

Amount of groups on HA (mmol/g)			
Carboxyl	Lactone	Phenol	Total
0.9604	0.0130	0.0780	1.0514

carboxyl group. The peak locating at 1070 cm⁻¹ may be owing to stretching of carbohydrate or alcoholic bonds (C-O-C or C-O). The wavenumbers ranging from 900 to 700 cm⁻¹ might inform plane vibrations of aromatic C-H, benzene and alkyl benzene bonds. In addition, to demonstrate the morphologies of HA, the typical SEM and TEM images were presented in Fig.S-1 and Fig S-2 (Electronic Supplement Information, ESI), It is observed that HA exhibits as lamellar sheets with disordered pores, which will facilitate the mass transfer as well as the occurrence of redox reactions.

To further confirm HA's chemical composition, the X-ray photoelectron spectroscopy (XPS) measurements and Boehm's titration analysis were conducted. As shown in the wide scan XPS spectrum (Fig. 2a), two typical peaks with the binding energy of 285 eV and 533 eV are easily indexed to C_{1s} and O_{1s} orbits respectively, indicating the main composition of carbon and oxygen elements. In addition, after de-convolution the complex C_{1s} spectrum (Fig. 2b) is divided into 4 different types of carbon species: C=C-C (284.6 eV, 69.7% mass ratio), C-O (286.4 eV, 17.6%), C=O (287.7 eV, 4.7%) and O-C=O (288.7 eV, 8%) groups, respectively¹³. Furthermore, as shown in Table 1, a large number of acidic groups, such as carboxyl, lactones, and phenolic, are detected during Boehm's titration analysis,¹⁴ accordant with the FTIR and XPS investigations. As a consequence, the combinational investigations of FTIR, XPS and Boehm's titration solidify the abundant existence of oxygenic functional groups in HA molecule and imply potential application for ion accumulation.

To evaluate the electrochemical performance for ions storages, cyclic voltammograms (CVs) were performed by using a half cell system where HA was used for the working electrode, and metal foils (lithium or sodium) acted as both the reference electrodes and the counter ones, respectively (Experimental information, ESI†). As depicted in Fig. 3a, HA presents a reduction peak centred at 1.06 V (vs Li/Li⁺) during the cathodic scan from 3 V to 0 V, informing the accumulating process of lithium ions. In the meanwhile, an anodic peak located at 0.82 V (vs Li/Li⁺) is observed, indicating the de-intercalation of lithium ions. Similarly, HA possesses the same sodium ion insertion process as that of Lithium-ion. As can be seen from the CV curves of Fig. 3b, HA displays one reduction peak centred at 0.71 V (vs Na/Na⁺) during the cathodic scan,

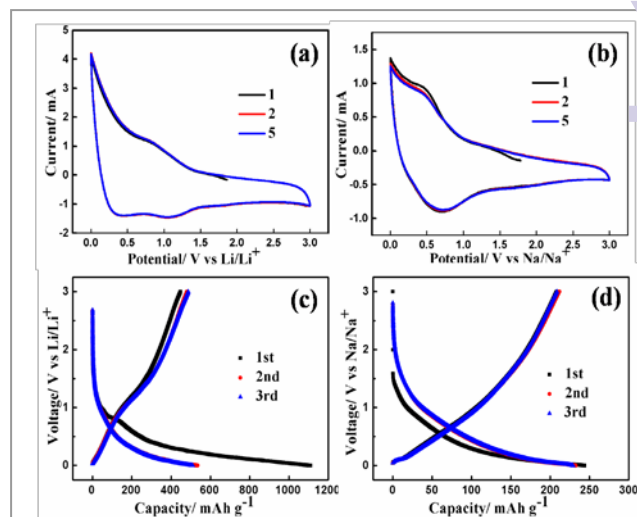
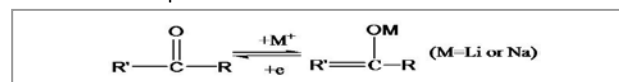


Fig.3 (a) The CV curves of HA in 1 M LiPF₆+EC+EMC+DMC (1:1 volume ratio), potential range: 0-3 V (vs Li), scan rate: 1 mV s⁻¹; (b) the CV curves of HA in 1 M NaPF₆+PC+DMC (1:1 volume ratio) electrolyte, scan rate: 1 mV s⁻¹, potential range: 0-3 V (vs Na); (c) the charge/discharge profiles of HA in a voltage range of 0-3 V (vs Li) at a constant current density of 20 mA g⁻¹; (d) the charge/discharge profiles of HA in a voltage range of 0-3 V (vs Na) at a constant current density of 20 mA g⁻¹.

corresponding to the insertion of Na-ions. The anodic scan shows an oxidation peak at 0.48 V (vs Na/Na⁺), which reveals the de-insertion of sodium ions. These comparatively reversible redox pairs at the low potential range (0-2V) validated the potential utilization of HA for lithium ions and sodium ions storage.¹⁵ Furthermore, it is observed that the current intensity of the reduction peak is nearly equal to that of the oxidation peak, suggesting the comparative reversible reactions occur for lithium ion intercalation/de-intercalation. Most interestingly, no obvious shift or shrinkage phenomena are observed during the first five cycles, indicating the probably cycling stability. To further elucidate the ion storage mechanism, the charged samples were compared and detected by FTIR spectrum technology. As recorded in Fig. S-3 (ESI), after the insertion of ions, several strong adsorption peaks (900-700 cm⁻¹ (benzene rings), 1300-1500 cm⁻¹ (C-O-C), 1600-1700 cm⁻¹ (C=C)) appear, implying the polarization and ionization effect of HA. Combining with other reports,⁶⁻¹⁰ it is deduced that the carboxyl groups might contribute to the observed capacity dominantly, which can be expressed as below:



In summary, both the CV curves and FTIR spectra presented imply that HA would be quite suitable for using as anode materials for both LIBs and SIBs.

To further evaluate the storage performance of HA, the galvanostatic charge/discharge technologies were conducted. Fig. 3c depicts discharge/charge profiles of the first three cycles of HA for lithium ions in the potential range 3-0 V vs Li⁺/Li at a current density of 20 mA g⁻¹. In the first discharge process, the voltage dropped sharply to 1.2 V and then experienced a long and gentle slope from 1.2 V to 0 V, corresponding to a capacity of 1100 mAh g⁻¹. Then the subsequent charge released a capacity of 484 mAh g⁻¹ with

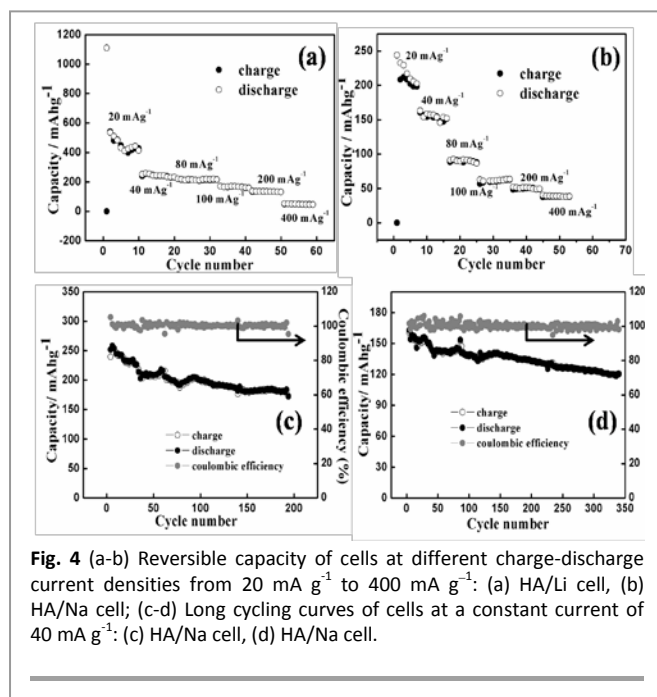


Fig. 4 (a-b) Reversible capacity of cells at different charge-discharge current densities from 20 mA g⁻¹ to 400 mA g⁻¹: (a) HA/Li cell, (b) HA/Na cell; (c-d) Long cycling curves of cells at a constant current of 40 mA g⁻¹: (c) HA/Na cell, (d) HA/Na cell.

an initial coulombic efficiency (CE) of 46%. This irreversible capacity loss might arise from the formation of solid electrolyte interphase (SEI) which is a common phenomenon for anode materials of LIBs at the first cycle.^{10a} After the first cycle, the lithium ions insertion and extraction process becomes relatively reversible with a capacity of 450 mAh g⁻¹ and a high CE of 92%. On the contrary, HA in SIBs (Fig. 3d) exhibits a discharge capacity of 244 mAh g⁻¹, a quasi-reversible charge capacity of 208.3 mAh g⁻¹ as well as an initial CE of 86% (higher than that of LIBs) in the first cycle. After that, the discharge/charge profile becomes constant with a CE of 95%. In summary, HA displays a higher capacity for LIBs than that of SIBs with an inferior CE.

Furthermore, the rate performances of HA in LIBs and SIBs were also evaluated. Fig. 4a records a comparison of electrochemical cycling performances of HA for lithium ions at different current densities (20–400 mA g⁻¹). It is observed that HA delivers stable capacities of 420 mAh g⁻¹ at 20 mA g⁻¹ and 60 mAh g⁻¹ at 400 mA g⁻¹ respectively. Similarly, the capacities of HA decrease gently from 220 mAh g⁻¹ to 40 mAh g⁻¹ for sodium-ion accumulation with the increase of the current densities (20–400 mA g⁻¹, Fig. 4b). It indicates that HA displays better rate capability in Li-ion electrolytes than that in Na-ion electrolytes, which may result from the size difference of Li-ion and Na-ion.¹⁵ In addition, the long cycling performance at a current density of 40 mA g⁻¹ was also studied in Li-ion and Na-ion electrolytes (Fig. 4c and 4d). After 200 cycles, discharge capacities of 180 and 133 mAh g⁻¹ were presented for LIBs and SIBs, corresponding to capacity retentions of 70% and 80%, respectively. Impressively, comparing to other referred small organic molecules,^{7,9} these enhancements in capacity retention might arise from the fact that the polymeric structure of HA would partly inhibited the dissolving of HA in organic electrolytes.¹¹⁶ Moreover, the CEs of the HA electrodes are more than 98% after the second cycle both for Li-ion and Na-ion storage at this current density. Collectively, the combination of abundant functional

groups with the polymeric framework endows HA with excellent storage performances not only for LIBs and SIBs.

In summary, combining the chemical analysis with electrochemical characterizations, HA has been successfully validated as promising anode materials for LIBs and SIBs, in which the abundance of functionalities in framework endows HA with high storage capacities, the polymeric structure satisfies HA with excellent cycling stabilities. Furthermore, it is envisioned this pioneering work not only paves a sustainable and effective strategy for developing organic energy storage devices, but also triggers researchers' interest in material exploration especially from renewable nature source.

This work was financially supported by the NSFC of China (21435005, 21403295 and U1303191), the "Western Light Foundation of Chinese Academy of Sciences (XBBS201320) and the Young Creative Sci-Tech Talents Cultivation Project of Xinjiang Uygur Autonomous Region (2013731024).

Notes and references

- (a) Z. P. Song and H. S. Zhou, *Energy Environ. Sci.*, 2013, **6**, 2280; (b) Y. Liang, Z. Tao, J. Chen, *Adv. Energy Mater.*, 2012, **2**, 742; (c) D. Larcher and J. M. Tarascon, *Nat. Chem.*, 2015, **7**, 19–29.
- (a) T. Sarukawa, and N. Oyama, *J. Electrochem. Soc.*, 2010, **157**, F23; (b) J. Y. Zhang, Z. P. Song, L. Z. Zhan, J. Tang, H. Zhan, Y. H. Zhou, and C. M. Zhan, *J. Power Sources*, 2009, **18**, 496.
- (a) T. Suga, H. Ohshiro, S. Sugita, K. Oyaizu and H. Nishida, *Adv. Mater.*, 2009, **21**, 1627; (b) W. Choi, S. Ohtani, K. Oyaizu, H. Nishida and K. E. Geckeler, *Adv. Mater.*, 2011, **23**, 4440; (c) W. Guo, Y. X. Yin, S. Xin, Y. G. Guo and L. J. Wan, *Energy Environ. Sci.*, 2012, **5**, 5221.
- (a) M. Zhou, J. F. Qian, X. P. Ai and H. X. Yang *Adv. Mater.*, 2011, **23**, 4913; (b) K. S. Park, S. B. Schougarrd and J. B. Goodenough, *Adv. Mater.*, 2007, **19**, 848.
- (a) H. Chen, M. Armand, G. Demailly, F. Dolhem, P. Poizat and J. M. Tarascon, *Chemsuschem*, 2008, **1**, 348; (b) S. Renault, J. Q. Geng, F. Dolhem and P. Poizat, *Chem. Commun.*, 2011, **47**, 2414.
- (a) M. Armand, S. Grugeon, H. Vezin, S. Laruelle, P. Ribiere, P. Poizat and J. M. Tarascon, *Nat. Mater.*, 2009, **8**, 120.
- (a) N. Ogihara, T. Yasuda, Y. Kishida, T. Ohsuna, K. Miyamoto, and N. Ohba, *Angew. Chem. Int. Ed.*, 2014, **53**, 11467; (b) T. Yasuda and N. Ogihara, *Chem. Commun.*, 2014, **50**, 11565.
- A. Abouimrane, W. Weng, H. Eltayeb, Y. Cui, J. Niklas, C. Poluektov and K. Amine, *Energy Environ. Sci.*, 2012, **5**, 9632.
- (a) L. Zhao, J. Zhao, Y. S. Hu, H. Li, Z. Zhou, M. Armand and J. Chen, *Adv. Energy Mater.*, 2012, **2**, 962; (b) Y. Park, D. S. Shin, S. H. Woo, N. S. Choi, K. H. Shin, S. M. Oh, K. T. Lee and S. Y. Hong, *Adv. Mater.*, 2012, **24**, 3562.
- (a) S. Wang, L. Wang, K. Zhang, Z. Zhu, Z. Tao, and J. Chen, *Nano Lett.*, 2013, **13**, 4404–4409; (b) S. Wang, L. Wang, Z. Zhu, Z. Hu, Q. Zhao and J. Chen, *Angew. Chem. Int. Ed.*, 2013, **53**, 5892.
- (a) Y. Jiao, D. Zhang, J. Zhao, X. Wang, H. Zhu and C. Wang, *Electrochim. Acta*, 2014, **136**, 504; (b) H. Zhu, J. Yin, X. Wang, H. Wang and X. Yang, *Adv. Funct. Mater.*, 2013, **23**, 1305; (c) H. Zhu, X. Wang, F. Yang and X. Yang, *Adv. Mater.* 2011, **23**, 2745.
- (a) F. J. Stevenson, *Humus chemistry: genesis, composition, reactions*, John Wiley & Sons, New York, 1994; (b) E. A.

COMMUNICATION

Journal Name

- Ghabbour and G. Davies, *Humic substances: structures, models and functions*, RSC publishing, Cambridge, U.K., 2001.
- 13 J. F. Moulder, W. F. Stickle, P. E. Sobel and K. D. Bomben, *Handbook of X-Ray Photoelectron Spectroscopy - A Reference Book of Standard Spectra for Identification and Interpretation of XPS Data*, Perkin-Elmer Corporation, Eden Prairie, MN, USA 1992.
- 14 H. P. Boehm, *Carbon*, 1994, 32, 759.
- 15 (a) R.R. Zhao, Y.L. Cao, X.P. Ai and H.X. Yang, *J Electroanal Chem.*, 2013, **688**, 93; (b) C. Wang, Y. Xu, Y. Fang, M. Zhou, L. Liang, S. Singh, H. Zhao, A. Schober, and Y. Lei, *J. Am. Chem. Soc.*, 2015, **137**, 3124.
- 16 (a) H. Pan, Y. Hu and L. Chen, *Energy Environ. Sci.*, 2013, **6**, 2338; (b) K. Wasinski, M. Walkowiak and G. Lota, *J Power Sources*, 2014, **255**, 230-234.

ChemComm Accepted Manuscript